DELFT UNIVERSITY OF TECHNOLOGY

REPORT 03-14

SOLUTION OF VECTOR STEFAN PROBLEMS WITH CROSS-DIFFUSION

F.J. VERMOLEN AND C. VUIK

ISSN 1389-6520

Reports of the Department of Applied Mathematical Analysis

Delft 2003

Solution of vector Stefan problems with cross-diffusion

F.J. Vermolen [1], C. Vuik

Delft University of Technology, *Department of Applied Mathematical Analysis*,
Mekelweg 4, 2628 CD Delft, the Netherlands

Abstract

A general model for the dissolution of particles in multi-component alloys is proposed and analyzed. The model is based on diffusion equations with cross-terms for the several species, combined with a Stefan condition as the equation of motion of the interface between the particle and diffusant phase. To facilitate the analysis we use a diagonalization argument or Jordan factorization for the diffusion matrix. Self-similar solutions with the Boltzmann transformation are derived to get insight into qualitative behavior of the solution and for comparison with numerical solutions. Several numerical schemes for the solution of the Stefan problem are proposed and compared. It turns out that diagonalization is usefull for numerical purposes too. However, for the case of position dependent diffusion coefficients or a non diagonalizable diffusion matrix, one has to use a different scheme. Here, we analyze stability and workload of several time integrations.

Keywords: Multi-component alloy, Particle dissolution, Cross-diffusion, Vector-valued Stefan problem, Self-similar solution

1 Introduction

In the thermal processing of both ferrous and non-ferrous alloys, homogenization of the as-cast microstructure by annealing at such a high temperature that unwanted precipitates are fully dissolved, is required to obtain a microstructure suited to undergo heavy plastic deformation as an optimal starting condition for a subsequent precipitation hardening treatment. Such a homogenization treatment, to name just a few examples, is applied in hot-rolling of Al killed construction steels, HSLA steels, all engineering steels, as well as aluminum extrusion alloys. Although precipitate dissolution is not the only metallurgical process taking place, it is often the most critical of the occurring processes. The minimum temperature at which the annealing should take place can be determined from thermodynamic analysis of the phases present. The minimum annealing time at this temperature, however, is not a constant but depends on particle size, particle geometry, particle concentration, overall composition etc.

Due to the scientific and industrial relevance of being able to predict the kinetics of particle dissolution, many models of various complexity [25, 14, 10, 35, 3, 23, 22, 27, 12, 1, 26, 15, 24, 34, 7, 21, 11, 2] have been presented and experimentally validated. In recent years the simpler models covering binary and ternary alloys have been extended

[1] corresponding author, e-mail: F.J.Vermolen@math.tudelft.nl

to cover multi-component particles [29, 31, 30]. These advanced models cover a range of physical assumptions concerning the dissolution conditions and the initial microstructure. Furthermore, mathematical implications (such as a possible bifurcation of the solution, monotonicity of the solution and well-posedness) are addressed and mathematically sound extensions to the case of n compound particles, with proven theorems concerning existence of mass-conserving solutions and solution bounds, have been derived.

In the current paper we formulate the model for particle dissolution in multi-component alloys in which cross-diffusion of the alloying elements is taken into account. Using diagonalization, we show that the case of cross-diffusion can be formulated similarly to the case where no cross-diffusion takes place, only the thermodynamic relation for the interfacial (equilibrium) concentrations changes. We give asymptotic solutions for the dissolution of a planar particle. We show that under certain circumstances the multi-component problem (a 'vector-valued' Stefan problem) can be approximated by a binary problem ('scalar' Stefan problem). Furthermore, we formulate several numerical methods to solve the cross-diffusion problem of which we compare its stability and workload. We show that the diagonalization, if applicable, is very usefull for numerical purpose too.

2 The model

The as-cast microstructure is simplified into a representative cell containing the 'matrix' of phase α and a single particle of phase β of a specific form, size and location of the cell boundary. The boundary between the β-particle and α-phase is referred to as the interface. Particle dissolution is assumed to proceed by a number of the subsequent steps [12, 26]: decomposition of the particle, atoms from the particle crossing the interface and diffusion of these atoms in(to) the α-phase. Here we take the effects of cross-diffusion into account. We assume in this work that the first two mechanisms proceed sufficiently fast with respect to diffusion. Hence, the interfacial concentrations are those as predicted by thermodynamics (local equilibrium).

In [30] we considered the dissolution of a stoichiometric particle in a ternary alloy. The hyperbolic relationship between the interfacial concentrations for ternary alloys is derived using a three-dimensional Gibbs space. For the case that the particle consists of n chemical elements apart from the atoms that form the bulk of the β-phase, a generalization to an n-dimensional Gibbs hyperspace has to be made. The Gibbs surfaces become hypersurfaces. We expect that similar consequences follow and that hence the hyperbolic relation between the interfacial concentrations remains valid for the general stoichiometric particle in a multi-component alloy. We denote the chemical species by Sp_i, $i \in \{1, ..., n+1\}$. We denote the stoichiometry of the particle by $(Sp_1)_{m_1}(Sp_2)_{m_2}(Sp_3)_{m_3}(...)(Sp_n)_{m_n}$. The numbers $m_1, m_2, ...$ are stoichiometric constants. We denote the interfacial concentration of species i by c_i^{sol} and we use the following hyperbolic relationship for the interfacial concentrations:

$$(c_1^{\mathrm{sol}})^{m_1}(c_2^{\mathrm{sol}})^{m_2}(...)(c_n^{\mathrm{sol}})^{m_n} = K = K(T). \tag{1}$$

The factor K is referred to as the solubility product and depends on temperature T.

The position of the moving interface between the β-particle and α-phase is denoted by $S(t)$. Consider a one-dimensional domain, i.e. there is one spatial variable, which extends from 0 up to M (the cell size). For cases of low overall concentrations in the alloy, the cell size M may be large and the solution resembles the case where M is infinite. The spatial co-ordinate is denoted by r, $0 \leq S(t) \leq r \leq M$. This domain is referred to as $\Omega(t) := \{r \in \mathbb{R} : S(t) \leq r \leq M\}$. The α-phase where diffusion takes place is given by $\Omega(t)$ and the β-particle is represented by the domain $0 \leq r < S(t)$. Hence for each alloying element, we have for $r \in \Omega(t)$ and $t > 0$ (where t denotes time)

$$\frac{\partial c_i}{\partial t} = \sum_{j=1}^{n} \frac{D_{ij}}{r^a} \frac{\partial}{\partial r} \left\{ r^a \frac{\partial c_j}{\partial r} \right\}, \text{ for } i \in \{1, ..., n\}. \tag{2}$$

Above equations follow from thermodynamic considerations, their derivation can for instance be found in [13, 10]. Here D_{ij} and c_i respectively denote the coefficients of the diffusion matrix and the concentration of the species i in the α-rich phase. This relaxes the assumption that the alloying elements diffuse independently. When cross-diffusion is neglected, the diffusion matrix is diagonal. The geometry is planar, cylindrical and spherical for respectively $a = 0, 1$ and 2. Let c_i^0 denote the initial concentration of each element in the α phase, i.e. we take as initial conditions (IC)

$$(IC) \begin{cases} c_i(r, 0) = c_i^0(r) \text{ for } i \in \{1, ..., n\} \\ \\ S(0) = S_0. \end{cases}$$

At a boundary not being an interface, i.e. at M or when $S(t) = 0$, we assume no flux through it, i.e.

$$\frac{\partial c_i}{\partial r} = 0, \text{ for } i \in \{1, ..., n\}. \tag{3}$$

Furthermore at the moving interface $S(t)$ we have the 'Dirichlet boundary condition' c_i^{sol} for each alloying element. The concentration of element i in the particle is denoted by c_i^{part}, this concentration is fixed at all stages (see Reiso et al [21]). The dissolution rate (interfacial velocity) is obtained from a mass-balance of the atoms of alloying element i. For $t > 0$ and $i, j \in \{1, ..., n\}$, the mass-balance per unit area leads to:

$$\left.\begin{array}{l} c_i(S(t), t) = c_i^{\text{sol}} \\ \\ \left(c_i^{\text{part}} - c_i^{\text{sol}}\right) \dfrac{dS}{dt} = \displaystyle\sum_{j=1}^{n} D_{ij} \frac{\partial c_j}{\partial r}(S(t), t) \end{array}\right\} \Rightarrow \sum_{k=1}^{n} \frac{D_{ik}}{c_i^{\text{part}} - c_i^{\text{sol}}} \frac{\partial c_k}{\partial r}(S(t), t) = \sum_{k=1}^{n} \frac{D_{jk}}{c_j^{\text{part}} - c_j^{\text{sol}}} \frac{\partial c_k}{\partial r}(S(t), t). \tag{4}$$

The right-hand part of above equations follows from local mass-conservation of the components. Above formulated problem falls within the class of Stefan-problems, i.e. diffusion

with a moving boundary. Since we consider simultaneous diffusion of several chemical elements, it is referred to as a 'vector-valued Stefan problem'. The unknowns in above equations are the concentrations c_i, interfacial concentrations c_i^{sol} and the interfacial position $S(t)$. All concentrations are non-negative. The coupling exists in both the diffusion equations, equation of motion and the values of the concentrations at the interfaces between the particle and α-rich phase. This strong coupling complicates the qualitative analysis of the equations. For a mathematical overview of Stefan problems we refer to the textbooks of Crank [8], Chadam and Rasmussen [5] and Visintin [33].

3 Qualitative remarks and analytical solutions

In this section we first diagonalize the diffusion matrix to facilitate the analysis of the equations. Subsequently, we show that the concentration profiles do not necessarily satisfy the maximum principle. Finally, similarity solutions and asymptotic solutions are given and motivated. These solutions are used for validation of the numerical scheme.

3.1 The vector-valued Stefan problem: decomposition of the diffusion matrix

Subsequently, we change into a vector notation of the equations. We define the vectors $\underline{c} := (c_1, c_2, \dots\ c_n)^T$, $\underline{c}^p := (c_1^{\text{part}}, c_2^{\text{part}}, \dots\ , c_n^{\text{part}})^T$, $\underline{c}^s := (c_1^{\text{sol}}\ c_2^{\text{sol}}\ \dots\ , c_n^{\text{sol}})^T$, then the diffusion equations become in vector notation

$$\frac{\partial}{\partial t}\underline{c} = \frac{1}{r^a}\frac{\partial}{\partial r}\left\{ r^a D \frac{\partial}{\partial r} \right\} \underline{c}. \tag{5}$$

The equation of motion of the interface becomes in vector notation:

$$(\underline{c}^p - \underline{c}^s)\,\frac{dS}{dt} = \frac{\partial}{\partial r} D\underline{c}(S(t), t).$$

Since we assume that D is constant, it is convenient for the analysis of equation (5) to look at a decomposition of the diffusion matrix D. Therefore we use the Decomposition Theorem in linear algebra, which says that for each $D \in \mathbb{R}^{n\times n}$ there exists a non-singular $P \in \mathbb{R}^{n\times n}$ such that $\Lambda = P^{-1}DP$, where Λ represents a Jordan block-matrix (see for instance Birkhoff and MacLane [4]). For cases where D has n independent eigenvectors, i.e. D is diagonalizable, Λ is diagonal with the eigenvalues of D on the main diagonal. Further, the columns of the matrix P consists of the eigenvectors of D. In the more general case of a Jordan decomposition we have that the matrix P consists of the generalized eigenvectors of D, which are obtained from solution of

$$(D - \lambda I)\underline{w}_{i+1} = \underline{w}_i, \text{ with } \underline{w}_1 = \underline{v},$$

where $I \in \mathbb{R}^{n\times n}$ is the identity matrix and $\underline{v}$ and $\underline{w}_i$ are an eigenvector and generalized eigenvectors of D respectively, belonging to the eigenvalue λ whose geometric multiplicity is less than the algebraic multiplicity. For the coming we assume that the eigenvalues are real. Substitution of the decomposition of D into Eq.(5) and using that D is constant gives

$$\frac{\partial}{\partial t}\underline{c} = \frac{1}{r^a}\frac{\partial}{\partial r}\left\{r^a \frac{\partial}{\partial r}\right\} P\Lambda P^{-1}\underline{c} \Leftrightarrow \frac{\partial}{\partial t}P^{-1}\underline{c} = \frac{1}{r^a}\frac{\partial}{\partial r}\left\{r^a \frac{\partial}{\partial r}\right\} \Lambda P^{-1}\underline{c}$$

$$(\underline{c}^p - \underline{c}^s)\frac{dS}{dt} = \frac{\partial}{\partial r}P\Lambda P^{-1}\underline{c}(S(t),t) \Leftrightarrow P^{-1}(\underline{c}^p - \underline{c}^s)\frac{dS}{dt} = \frac{\partial}{\partial r}\Lambda P^{-1}\underline{c}(S(t),t).$$

We define the transformed concentrations as

$$\begin{array}{ll} \underline{u} := P^{-1}\underline{c}, & \underline{u}^s := P^{-1}\underline{c}^s \\ \underline{u}^p := P^{-1}\underline{c}^p, & \underline{u}^0 := P^{-1}\underline{c}^0 \end{array}$$

then the diffusion equation and equation of motion change into

$$\begin{aligned} \frac{\partial}{\partial t}\underline{u} &= \frac{1}{r^a}\frac{\partial}{\partial r}\left\{r^a \frac{\partial}{\partial r}\right\} \Lambda\underline{u} \\ (\underline{u}^p - \underline{u}^s)\frac{dS}{dt} &= \frac{\partial}{\partial r}\Lambda\underline{u}(S(t),t). \end{aligned} \tag{6}$$

Above equations involve Jordan matrices with the eigenvalues of the diffusion matrix. For non-defective matrices the matrix in the above expressions is diagonal and the system is fully uncoupled. The homogeneous Neumann conditions at the non-moving boundary are similar for the transformed concentrations due to the linear nature of the transformation. Further, we have for $t = 0$

$$u_j = \begin{cases} u_j^0, & \text{for } x \in \Omega(0), \\ & \qquad\qquad j \in \{1,\ldots,n\} \\ u_j^{\text{part}}, & \text{for } x \in [0,M]\setminus\Omega(0). \end{cases} \tag{7}$$

From the decomposition of the diffusion matrix, with $\underline{c} = P\underline{u} \Rightarrow c_i = \sum_{j=1}^{n} p_{ij}u_j$, the coupling between the interfacial concentrations via the hyperbolic relation (1) changes into

$$(\sum_{j=1}^{n} p_{1j}u_j^s)^{m_1}(\sum_{j=1}^{n} p_{2j}u_j^s)^{m_2}(\ldots)(\sum_{j=1}^{n} p_{nj}u_j^s)^{m_n} = K = K(T). \tag{8}$$

Although this condition becomes more complicated, the analysis is facilitated using the diagonalization of the diffusion matrix.

In the Jordan-matrix we have one uncoupled concentration for each eigenvalue of D.

This implies that whenever one eigenvalue is negative, an uncoupled diffusion equation with a negative diffusivity results for the decomposed system. In other words, we face the following equation

$$\frac{\partial u_i}{\partial t} = -\mu \frac{1}{r^a} \frac{\partial}{\partial r} \left\{ r^a \frac{\partial u_i}{\partial r} \right\}, \text{ with } \mu := -\lambda < 0, \text{ for } x \in \Omega(t), t > 0.$$

It is well-known that the above equation is unstable with respect to perturbations and hence the problem is ill-posed. This motivates the requirement that the eigenvalues of the diffusion matrix have to be positive.

3.2 Violation of the maximum principle

For the case of non-coupled diffusion equation it is well-known that solutions of diffusion equations satisfy a maximum principle. Therefore, after diagonalization, the transformed concentrations satisfy this maximum principle as well. We will show in this section that the transformed concentrations possibly violate the maximum principle. This will be treated for the case that the boundaries do not move. An extension with a moving boundary can be made with the self-similar solution for a moving boundary, which is presented later.

We explain this for the ternary case, i.e. $D \in \mathbb{R}^{2\times 2}$, first with non-moving boundaries. In Section 3 we will treat the case where the boundary moves. The Jordan decomposition then gives

$$\Lambda = \begin{pmatrix} \lambda & 1 \\ 0 & \lambda \end{pmatrix}.$$

Hence the system of two equations is reduced to for $x \in (0,1), t > 0$:

$$\begin{cases} \dfrac{\partial u_2}{\partial t} = \lambda \dfrac{\partial^2 u_2}{\partial x^2} \\ \dfrac{\partial u_1}{\partial t} = \lambda \dfrac{\partial^2 u_1}{\partial x^2} + \dfrac{\partial^2 u_2}{\partial x^2}. \end{cases} \tag{9}$$

We consider smooth solutions of the above equations in the sense of

$$(S): \qquad u_1, u_2 \in C^{2,1}((0,1)\times\mathbb{R}^+) \cap C^{1,0}([0,1]\times\mathbb{R}_0^+).$$

Furthermore, let us consider the following boundary- and initial conditions

$$(IBC) \begin{cases} u_2(0,t) = u_2^s, \quad u_1(0,t) = u_1^s, \\ u_2(x,0) = u_2^0, \quad u_1(x,0) = u_1^0, \\ \dfrac{\partial u_1}{\partial x}(1,t) = 0, \quad \dfrac{\partial u_2}{\partial x}(1,t) = 0. \end{cases}$$

The solution of the first equation in (9) satisfies a maximum principle, i.e. u_2 has no extreme for $x \in (0,1)$ and $t > 0$. A proof of this fact is given by Protter and Weinberger [20]. Since u_2 satisfies a maximum principle and a homogeneous Neumann boundary condition at $x = 1$, it follows that u_2 is concave-upward or concave-downward whenever $u_2^s > u_2^0$ or $u_2^s < u_2^0$ respectively, i.e.

$$\frac{\partial^2 u_2}{\partial x^2} > 0, \text{ whenever } u_2^s > u_2^0; \text{ and } \frac{\partial^2 u_2}{\partial x^2} < 0, \text{ whenever } u_2^s < u_2^0.$$

For the function u_1 we will show that an interior minimum cannot exist for any $x \in (0,1)$, $t > 0$ whenever $u_2^s > u_2^0$ and similarly an interior maximum cannot exist whenever $u_2^s < u_2^0$:

Proposition 1 *Let the functions u_2 and u_1 satisfy equations* (9) *and smoothness condition (S) with initial and boundary conditions (IBC), then*

1. *no internal minimum exists for u_1 whenever u_2 is concave-upward,*
2. *no internal maximum exists for u_1 whenever u_2 is concave-downward.*

Proof: Since u_2 and u_1 are smooth, it follows that an internal extreme, say for $(x,t) = (\hat{x},\hat{t}) \in (0,1) \times \mathbb{R}^+$ is necessarily a stationary point, i.e. for u_1 this gives $\frac{\partial u_1}{\partial t} = 0 = \frac{\partial u_1}{\partial x}$ for $(x,t) = (\hat{x},\hat{t})$. Furthermore, for an extreme at $(\hat{x},\hat{t})$ to be an internal (local) minimum we must have $\frac{\partial^2 u_1}{\partial x^2}(\hat{x},\hat{t}) \geq 0$ and similarly for an internal (local) maximum we have $\frac{\partial^2 u_1}{\partial x^2}(\hat{x},\hat{t}) \leq 0$. For any stationary point $(\hat{x},\hat{t})$ for u_1 we obtain from (9)

$$\lambda \frac{\partial^2 u_2}{\partial x^2} + \frac{\partial^2 u_1}{\partial x^2} = 0 \Leftrightarrow \lambda \frac{\partial^2 u_2}{\partial x^2} = -\frac{\partial^2 u_1}{\partial x^2} \text{ for } (x,t) = (\hat{x},\hat{t}).$$

Suppose that $\frac{\partial^2 u_2}{\partial x^2}(\hat{x},\hat{t}) > 0$, then $\frac{\partial^2 u_1}{\partial x^2}(\hat{x},\hat{t}) < 0$ and hence an internal minimum cannot exist for $(\hat{x},\hat{t})$. Since $\frac{\partial^2 u_2}{\partial x^2} > 0$ for $u_2^s > u_2^0$, an interior minimum cannot exist for u_1 when $u_2^s > u_2^0$ and the first part of Proposition 1 is proven, the proof of the second part of Proposition 1 is analogous. □

We will derive, for the case of a 'half-infinite' domain, a criterion for u_2^s and u_2^0 for the existence of an internal extreme. For this semi-unbounded domain $x > 0$ and $t > 0$ we consider self-similar solutions in the form of $u_2, u_1(x,t) = \overline{u_2}, \overline{u_1}(\eta)$, $\eta := \frac{x}{\sqrt{t}}$. For simplicity

we will take $u_2^0 = 0 = u_1^0$. Substitution into (9) implies

$$\begin{cases} -\frac{\eta}{2}\overline{u_2}' = \lambda\overline{u_2}'' \\ \\ -\frac{\eta}{2}\overline{u_1}' = \lambda\overline{u_2}'' + \overline{u_1}'' \end{cases} \tag{10}$$

Here we use as boundary conditions

$$(BC)\begin{cases} \overline{u_2}(0) = u_2^s, \quad \overline{u_1}(0) = u_1^s, \\ \\ \lim_{\eta\to\infty} u_2(\eta) = 0 = \lim_{\eta\to\infty} u_1(\eta). \end{cases}$$

For simplicity we set $f = f(\eta) = \overline{u_2}'$ and $g = g(\eta) = \overline{u_1}'$, then we obtain the following solution for f:

$$f = C_1 \mathrm{e}^{-\frac{\eta^2}{4\lambda}},$$

and for the function g we obtain the following linear differential equation:

$$g' + \frac{\eta}{2\lambda} g = \frac{\eta}{2\lambda^2} f$$

The above differential equation is solved using an integrating factor to obtain

$$g = \left(C_1 \frac{\eta^2}{4\lambda^2} + C_2 \right) \mathrm{e}^{-\frac{\eta^2}{4\lambda}}.$$

Integration of the functions f and g gives:

$$\overline{u_1} = C_1 \frac{1}{4\lambda^2} \int_0^\eta s^2 \mathrm{e}^{-\frac{s^2}{4\lambda}} ds + C_2 \int_0^\eta \mathrm{e}^{-\frac{s^2}{4\lambda}} ds + D_1$$

$$\overline{u_2} = C_1 \int_0^\eta \mathrm{e}^{-\frac{s^2}{4\lambda}} + D_2$$

By partial integration the integral in the upper equation is computed to yield

$$\overline{u_1} = \frac{C_1}{2\lambda^2} \left(-\eta\lambda \mathrm{e}^{-\frac{\eta^2}{4\lambda}} + \lambda\sqrt{\pi\lambda}\mathrm{erf}(\frac{\eta}{2\sqrt{\lambda}}) \right) + C_2\sqrt{\pi\lambda}\mathrm{erf}(\frac{\eta}{2\sqrt{\lambda}}) + D_1$$

$$\overline{u_2} = C_1\sqrt{\pi\lambda}\mathrm{erf}(\frac{\eta}{2\sqrt{\lambda}}) + D_2$$

The function $\overline{u_1}$ is monotonous whenever g does not change sign. Furthermore, $\overline{u_1}$ is monotonous if and only if u_1 is monotonous in space and time. Using the boundary

conditions the integration constants can be computed. For the function g then follows

$$g = g(\eta) = \overline{u_1}' = \left(\frac{1}{2} u_2^s - u_1^s - \frac{u_2^s}{4\lambda^2} \eta^2 \right) \frac{\mathrm{e}^{-\frac{\eta^2}{4\lambda^2}}}{\sqrt{\pi \lambda}}.$$

The above equation implies that $\overline{u_1}$ exhibits a (local) interior extreme whenever $\frac{1}{2} u_2^s - u_1^s > 0$. We summarize the result in Proposition 2:

Proposition 2 *Consider equations* (10) *for a semi-unbounded domain, supplemented with boundary conditions (BC), then the self-similar solution with* $u_2, u_1(x,t) = \overline{u_2}, \overline{u_1}(\eta)$, $\eta := \frac{x}{\sqrt{t}}$ *has an interior extreme whenever* $\frac{1}{2\lambda} u_2^s - u_1^s > 0$.

3.3 Similarity solutions and asymptotics

In this section we consider the Stefan problem in an unbounded domain. First we deal with the diagonalizable case where we consider an exact solution and an asymptotic approximation. Subsequently we deal with the non-diagonalizable case where we also consider an exact solution and an asymptotic approximation. Atkinson et al [2] use a slightly different procedure to derive a self-similar solution for the dissolution of stoichiometric particles in steel. The difference between their problem and our problem is the presence of two moving boundaries:

1. a boundary between the particle and the diffusant (in their case austenite),
2. a boundary between the diffusant and another phase in which diffusion is neglected (in their case ferrite).

There and in this paper a self-similar solution based on Boltzmann transformation is derived. Furthermore, in this paper we extend the solution to approximate solutions in terms of a quasi-binary approach if the particle concentrations are large compared to the other concentrations.

3.3.1 The exact solution of Neumann for the diagonalizable case

As an trial solution of equations (6) and (7) we assume that the interfacial concentrations $\underline{u}^s$ are constant. Furthermore, we assume that the diffusion matrix, D, is diagonalizable. Using a similar procedure as in [29], one obtains the solution for each component:

$$u_i = u_i^0 + (u_i^0 - u_i^s) \frac{\operatorname{erfc}(\frac{r - S_0}{2\sqrt{\lambda_i t}})}{\operatorname{erfc}(\frac{k}{2\sqrt{\lambda_i}})}, \qquad \text{for } i \in \{1, \ldots, n\}.$$

The assumption that $S = S_0 + k\sqrt{t}$ leads to the following problem to determine k and $\underline{u}^s$

$$(P_1)\begin{cases} \dfrac{u_i^0 - u_i^s}{u_i^p - u_i^s} \cdot \sqrt{\dfrac{\lambda_i}{\pi}} \cdot \dfrac{e^{-\frac{k^2}{4\lambda_i}}}{\operatorname{erfc}(\frac{k}{2\sqrt{\lambda_i}})} = \dfrac{k}{2}, & \text{for } i \in \{1,\ldots,n\}, \\ (\sum_{j=1}^{n} p_{1j}u_j^s)^{m_1}(\sum_{j=1}^{n} p_{2j}u_j^s)^{m_2}(\ldots)(\sum_{j=1}^{n} p_{nj}u_j^s)^{m_n} = K = K(T). \end{cases}$$

Here the unknowns are the transformed interfacial concentrations $\underline{u}^s$ and rate-parameter k. In above problem there is no time-dependence, hence the ansatz of time-independent transformed interfacial concentrations (and hence the physical interfacial concentrations) is not contradicted. Due to the non-linear nature of the equations, the solution is in general not unique. We apply numerical zero-point methods to obtain the solution. To get insight in the qualitative aspects of the solution, we consider some approximate solutions in the next subsubsection.

3.3.2 An asymptotic solution for the diagonalizable case

Suppose that $||\underline{u}^s - \underline{u}^0|| \ll ||\underline{u}^p - \underline{u}^s||$, then the solution of problem (P_1) can be approximated by the solution of

$$(P_2)\begin{cases} k = 2\dfrac{u_i^0 - u_i^s}{u_i^p - u_i^s}\sqrt{\dfrac{\lambda_i}{\pi}}, & \text{for } i \in \{1,\ldots,n\}, \\ (\sum_{j=1}^{n} p_{1j}u_j^s)^{m_1}(\sum_{j=1}^{n} p_{2j}u_j^s)^{m_2}(\ldots)(\sum_{j=1}^{n} p_{nj}u_j^s)^{m_n} = K = K(T). \end{cases}$$

Suppose that the initial concentrations are zero, then $\underline{u}^0 = \underline{0}$, further we assume that the transformed particle concentration is much larger than the transformed interfacial concentrations, i.e. $u_i^s \ll u_i^p$ for $i \in \{1,\ldots,n\}$, then it follows that the first equation of (P_2) becomes

$$k \approx 2\frac{u_1^s}{u_1^p}\sqrt{\frac{\lambda_1}{\pi}}. \tag{11}$$

Hence the equation of motion of the interface becomes

$$\frac{dS}{dt} \approx -\frac{u_1^s}{u_1^p}\sqrt{\frac{\lambda_1}{\pi t}}. \tag{12}$$

Further, the following recurrence relation between the transformed interfacial concentrations follows (see also [29], [32] for the derivation):

$$u_i^s = \frac{u_i^p}{u_1^p}\sqrt{\frac{\lambda_1}{\lambda_i}}u_1^s.$$

Substitution of above transformed interfacial concentrations into the second equation of (P_3) gives the following real-valued solution

$$u_1^s = \left(\frac{K}{\left(\sum_{j=1}^{n} p_{1j}\frac{u_j^p}{u_1^p}\sqrt{\frac{\lambda_1}{\lambda_j}}\right)^{m_1}\left(\sum_{j=1}^{n} p_{2j}\frac{u_j^p}{u_1^p}\sqrt{\frac{\lambda_1}{\lambda_j}}\right)^{m_2}(\ldots)\left(\sum_{j=1}^{n} p_{nj}\frac{u_j^p}{u_1^p}\sqrt{\frac{\lambda_1}{\lambda_j}}\right)^{m_n}} \right)^{\frac{1}{\mu}},$$

where we defined $\mu := \sum_{j=1}^{n} m_j$. Above expression for the transformed interfacial concentration is substituted into the rate equation for the interface (11). This gives

$$\frac{dS}{dt} = -\frac{1}{u_1^p}\left[\prod_{k=1}^{n}\frac{K}{\left(\sum_{j=1}^{n}\left(p_{kj}\frac{u_j^p}{u_1^p}\sqrt{\frac{\lambda_1}{\lambda_j}}\right)\right)^{m_k}}\right]^{\frac{1}{\mu}}\sqrt{\frac{\lambda_1}{\pi t}}.$$

In above equation we put the factors u_1^p and λ_1 out of the summation and product in the denominator. Furthermore subsequent multiplication of both the denominator and numerator by $\prod_{k=1}^{n}\left(\sqrt{\lambda_k}\right)^{1/\mu}$ gives

$$\frac{dS}{dt} = -\frac{c_{\text{eff}}^{\text{sol}}}{c_{\text{eff}}^{\text{part}}}\sqrt{\frac{D_{\text{eff}}}{\pi t}}, \tag{13}$$

where

$$c_{\text{eff}}^{\text{sol}} = K^{1/\mu},\ D_{\text{eff}} = \left[\prod_{i=1}^{n}(\lambda_k)^{m_i}\right]^{1/\mu},\ c_{\text{eff}}^{\text{part}} = \left[\prod_{k=1}^{n}\left(\sum_{j=1}^{n}\left(p_{kj}u_j^p\sqrt{\frac{\lambda_k}{\lambda_j}}\right)\right)\right]^{1/\mu}. \tag{14}$$

Above equation (14) gives the effective interfacial concentration, effective particle concentration and effective diffusivity. These quantities follow in terms of the solubility product, transformed particle concentrations and the eigenvalues and eigenvectors of the diffusion

matrix. The differential equation (13) is solved using separation of variables. Dissolution times of the particle can be determined then using known parameters such as the eigenvalues and eigenvectors of the diffusion matrix.

3.3.3 The exact solution of Neumann for the non-diagonalizable case

We deal with a ternary example, where $n = 2$. Examples with more chemical species can be treated similarly. When the matrix D is not diagonalizable then we obtain

$$\Lambda = \begin{pmatrix} \lambda & 1 \\ 0 & \lambda \end{pmatrix}$$

as the decomposed form of the diffusion matrix. The set of transformed diffusion equations become

$$\begin{cases} \dfrac{\partial u_1}{\partial t} = \lambda \dfrac{\partial^2 u_1}{\partial x^2} + \dfrac{\partial^2 u_2}{\partial x^2} \\ \dfrac{\partial u_2}{\partial t} = \lambda \dfrac{\partial^2 u_2}{\partial x^2} \end{cases} \tag{15}$$

From the above system it can be seen that the equation for u_2 is uncoupled. Its solution is computed using the self-similarity transformation and subsequently substituted into the equation for u_1. We consider self-similarity solutions $u_1, u_2(x,t) = \overline{u}_1\overline{u}_2, (\eta)$, where $\eta := \dfrac{x - S_0}{\sqrt{t}}$, then a similar procedure as in Section 3.4. the following is obtained:

$$\overline{u}_1 = \frac{C_1}{2\lambda^2}\left(-\eta\lambda \mathrm{e}^{-\frac{\eta^2}{4\lambda}} + \lambda\sqrt{\pi\lambda}\mathrm{erf}(\frac{\eta}{2\sqrt{\lambda}})\right) + C_2\sqrt{\pi\lambda}\mathrm{erf}(\frac{\eta}{2\sqrt{\lambda}}) + D_1$$

$$\overline{u}_2 = C_1\sqrt{\pi\lambda}\mathrm{erf}(\frac{\eta}{2\sqrt{\lambda}}) + D_2$$

Again we use the trial solution $S = S_0 + k\sqrt{t}$, a combination with the boundary conditions delivers

$$C_1 = \frac{u_2^0 - u_2^s}{\sqrt{\pi\lambda}\mathrm{erfc}(\frac{k}{2\sqrt{\lambda}})}, \qquad D_2 = u_2^0 - C_1\sqrt{\pi\lambda}$$

$$C_2 = \frac{1}{\sqrt{\pi\lambda}}\left\{\frac{u_1^0 - u_1^s}{\mathrm{erfc}(\frac{k}{2\sqrt{\lambda}})} - \frac{C_1}{2}\left(\sqrt{\frac{\pi}{\lambda}} + \frac{k}{\lambda}\frac{\mathrm{e}^{-\frac{k^2}{4\lambda}}}{\mathrm{erfc}(\frac{k}{2\sqrt{\lambda}})}\right)\right\}, \quad D_1 = u_1^0 - \sqrt{\pi\lambda}C_2 - \tfrac{C_1}{2}\sqrt{\tfrac{\pi}{\lambda}}.$$

Substitution of these constants into the expressions of u_1 and u_2 gives the transformed concentrations. Further, the rate factor of the interface movement is obtained from combination of the Stefan condition and the expression for u_2. Then we get the following set

of equations to be solved for k, u_1^s and u_2^s:

$$
\begin{aligned}
&(u_2^p - u_2^s)\frac{k}{2\sqrt{\lambda}} = \frac{u_2^0 - u_2^s}{\operatorname{erfc}(\frac{k}{2\sqrt{\lambda}})}\sqrt{\frac{1}{\pi}} \cdot \mathrm{e}^{-\frac{k^2}{4\lambda}} \\
&(u_1^p - u_1^s)\frac{k}{2\sqrt{\lambda}} = \frac{\mathrm{e}^{-\frac{k^2}{4\lambda}}}{\operatorname{erfc}(\frac{k}{2\sqrt{\lambda}})}\left\{(u_1^0 - u_1^s)\sqrt{\frac{1}{\pi}} + \frac{u_2^0 - u_2^s}{2\lambda\sqrt{\pi}} \cdot \left(1 + 2\frac{k^2}{4\lambda} - \frac{k}{2\sqrt{\lambda}}\frac{2}{\sqrt{\pi}}\frac{\mathrm{e}^{-\frac{k^2}{4\lambda}}}{\operatorname{erfc}(\frac{k}{2\sqrt{\lambda}})}\right)\right\} \\
&(p_{11}u_1^s + p_{12}u_2^s)^{m_1}\,(p_{21}u_1^s + p_{22}u_2^s)^{m_2} = K.
\end{aligned}
\tag{16}
$$

Note that $\underline{p}_1$ and $\underline{p}_2$ respectively represent the eigenvector and generalized eigenvector that correspond to the eigenvalue λ of the defective matrix D. In the next subsection we will consider some approximations of the solution of the above equations.

3.3.4 An asymptotic solution for the non-diagonalizable case

Suppose $|u_2^s - u_2^0| \ll |u_2^p - u_2^s|$, then $k \to 0$ and hence $\dfrac{\mathrm{e}^{-\frac{k^2}{4\lambda}}}{\operatorname{erfc}(\frac{k}{2\sqrt{\lambda}})} \to 1$. The above equations (16) tend to the following expressions:

$$
\begin{aligned}
\frac{k}{2\sqrt{\lambda}} &= \sqrt{\frac{1}{\pi}}\frac{u_2^0 - u_2^s}{u_2^p - u_2^s} \\
\frac{k}{2\sqrt{\lambda}} &= \sqrt{\frac{1}{\pi}}\left\{\frac{u_1^0 - u_1^s}{u_1^p - u_1^s} + \frac{u_2^0 - u_2^s}{2\lambda(u_1^p - u_1^s)}\right\}
\end{aligned}
\tag{17}
$$

As an approximation we set $u_i^0 \approx 0$ and $u_i^p \gg u_i^s$, then the above equation change into

$$
\begin{aligned}
k &= -2\sqrt{\frac{\lambda}{\pi}}\frac{u_2^s}{u_2^p} \\
k &= -2\sqrt{\frac{\lambda}{\pi}}\left\{\frac{u_1^s}{u_1^p} + \frac{u_2^s}{2u_1^p\lambda}\right\}
\end{aligned}
\tag{18}
$$

From the above equations, we obtain the following relation between u_1^s and u_2^s:

$$
u_2^s = \frac{u_2^p}{(u_1^p - \frac{u_2^p}{2\lambda})}u_1^s, \text{ for } u_1^p - \frac{u_2^p}{2\lambda} \neq 0.
$$

The above expression is substituted into the bottom equation of equation (16), which links u_1^s and u_2^s, to obtain a value for u_1^s. Using this value u_2^s can be computed and

subsequently we can compute the interface rate coefficient k. The interface movement can then be determined. Note from the above equation that the expression for the interfacial concentrations is less simple than for the case in which there is no cross-diffusion.

4 . Numerical method for the moving boundary problem

In general situations the vector-valued Stefan problems cannot be solved analytically. In order to obtain an approximation numerical methods can be used. The Stefan problems considered in this paper contain two problems:

- the computation of the moving interface;
- the occurrence of the cross-diffusion terms.

Our main interest is to give an accurate discretization of the boundary conditions for this Stefan problem with one spatial co-ordinate. For a survey of other methods, we refer to [25, 14, 19, 6, 9]. Therefore we use the classical moving grid method of Murray and Landis [17] to discretize the diffusion equations. In this paper we briefly describe the method, for more details we refer to [29]. In this section we first treat the stability of the numerical solution of the diffusion equations obtained from various time-integrations. Then, we treat a one-dimensional discretization of the vector-valued Stefan problem. Finally, we describe the solution of the cross-diffusion equations with the use of the diagonalization argument. The numerical performance of the methods is compared experimentally in the next section.

4.1 . Stability analysis of the Numerical method for the non-diagonalized diffusion equations

In this section we restrict ourselves to a vector cross diffusion problem with fixed boundaries. Two methods can be used. First if the diffusion matrix is constant the diagonalization argument can be used (see Section). If this assumption does not hold a numerical method for the coupled diffusion equations should be used. In the first method (with diagonalization) the stability properties of the time integration are well-known. In this section we investigate the stability properties for various time integration methods for the coupled equations. For the stability analysis we again assume that D is constant. Since, in future work we will compute the solution of the Stefan problem with cross-diffusion in more spatial dimensions by the use of Finite Elements, we keep the treatment as general as possible. Therefore, we consider the time integration of

$$\frac{\partial c_1}{\partial t} = D_{11}\Delta c_1 + D_{12}\Delta c_2, \tag{19}$$

$$\frac{\partial c_2}{\partial t} = D_{21}\Delta c_1 + D_{22}\Delta c_2, \tag{20}$$

Since the Laplacian operator is negative and self-adjoint, we assume that the discretization matrix for Δ, denoted by L, is symmetric and negative definite. Hence, its eigenvalues are negative. Further, we assume that the terms on the main diagonal of D are positive, i.e. $D_{11}, D_{22} > 0$ and $D \in \mathbb{R}^{2\times 2}$. Then, we write the discretized version as

$$\frac{\partial \underline{c}}{\partial t} = \begin{pmatrix} D_{11}L & D_{12}L \\ D_{21}L & D_{22}L \end{pmatrix} \begin{pmatrix} \underline{c}_1 \\ \underline{c}_2 \end{pmatrix} =: A\underline{c}, \tag{21}$$

where we use the following notation for N gridpoints:

$$\underline{c}_1 := \begin{pmatrix} c_{1,1} & c_{1,2} & \dots & c_{1,N} \end{pmatrix}^T, \underline{c}_2 := \begin{pmatrix} c_{2,1} & c_{2,2} & \dots & c_{2,N} \end{pmatrix}^T, \underline{c} = \begin{pmatrix} \underline{c}_1 \\ \underline{c}_2 \end{pmatrix}. \tag{22}$$

We observe that the matrix A in equation (21) represents a Kronecker product. For stability of eq. (20) we require that

$$\Re(eig(A)) < 0. \tag{23}$$

Note that eq. (20) falls into the class of Cauchy problems. Let λ be an eigenvalue of L and let μ be an eigenvalue of D, then $\mu\lambda$ is an eigenvalue of A. This assertion can for instance be found in Lancaster [16]. Since L is symmetric and only has negative (real-valued) eigenvalues, this implies in combination with eq. (23) that we should have

$$\Re(eig(D)) > 0, \tag{24}$$

in order to have that perturbations in the solution of equation (21) decrease if time increases.

Now we analyze the numerical stability of the following time integration methods for equation (21):

1. Euler Forward time integration,
2. Euler Backward time integration,
3. IMplicit EXplicit (IMEX) time integration.

We remark here that the stability analysis is based on the assumption that the eigenvalues of the discrete Laplacian are negative, i.e. $\lambda \in \mathbb{R}_-$. This is always true for a symmetric discretization. For finite element methods, it follows that the stiffness matrix (the discretized Laplacian) is always symmetric. However, equations (22) change due to the mass-matrix M that appears in the Finite Element formulation:

$$\begin{pmatrix} M & 0 \\ 0 & M \end{pmatrix} \frac{\partial \underline{c}}{\partial t} = \begin{pmatrix} D_{11}L & D_{12}L \\ D_{21}L & D_{22}L \end{pmatrix} \begin{pmatrix} \underline{c}_1 \\ \underline{c}_2 \end{pmatrix} =: A\underline{c}. \tag{25}$$

Since M is symmetric and assumed to be positive (diagonally dominance), the above

equation is re-written as

$$\frac{\partial \underline{c}}{\partial t} = \begin{pmatrix} D_{11}M^{-1}L & D_{12}M^{-1}L \\ D_{21}M^{-1}L & D_{22}M^{-1}L \end{pmatrix} \begin{pmatrix} \underline{c}_1 \\ \underline{c}_2 \end{pmatrix} =: A\underline{c}, \tag{26}$$

We use that L is symmetric negative definite and that M is symmetric positive definite (hence $M^{1/2}$ exists) to show that $M^{-1}L$ has negative (real-valued) eigenvalues. Since $M^{-1}L$ is similar to $M^{1/2}M^{-1}LM^{-1/2} = M^{-1/2}LM^{-1/2}$, it can be seen that the eigenvalues of $M^{-1}L$ are real-valued due to symmetry of $M^{-1/2}LM^{-1/2}$. Next we show that $M^{-1}L$ has negative eigenvalues only. Since $(Lx, x) < 0$ for all $x \neq 0$, we have $(LM^{-1/2}y, M^{-1/2}y) < 0$ for all $y \neq 0$ ($M^{-1/2}$ is non-singular). Since $M^{-1/2}$ is symmetric, it follows that $(M^{-1/2}LM^{-1/2}y, y) < 0$ for all $y \neq 0$. Combined with symmetry this gives that all eigenvalues of $M^{-1/2}LM^{-1/2}$ are negative. Hence, due to the similarity of $M^{-1}L$ to $M^{-1/2}LM^{-1/2}$, $M^{-1}L$ has negative (real-valued) eigenvalues only. This implies that the stability analysis also applies for Finite Element methods and that for Finite elements the matrix L in the treatment to follow should be replaced by $M^{-1}L$.

Euler Forward

The Euler Forward time integration method of equation (21) is given by

$$\underline{c}^{n+1} = (I + \Delta t A)\underline{c}^n. \tag{27}$$

If the eigenvalues of A are real, we obtain the following bound on Δt:

$$\Delta t < \frac{2}{|\lambda_1|\mu_1}, \tag{28}$$

where $|\lambda_1|$ and μ_1 respectively represent the maximum absolute value of $eig(L)$ and maximum value of $eig(D)$. For the case of finite differences with uniform gridsize h in one spatial dimension, Gerschgorin's Theorem delivers

$$\Delta t < \frac{h^2}{2\mu_1}. \tag{29}$$

This stability condition co-incides with the stability condition that is obtained if the diagonalization argument is combined with an explicit time integration. If $eig(D) \notin \mathbb{R}$, we obtain

$$(1 + \lambda\Delta t\alpha)^2 + (\lambda\Delta t\beta)^2 < 1, \text{ where } \mu = \alpha + i\beta, \tag{30}$$

as a necessary and sufficient condition for stability. Some elementary algebra reveals that the above condition co-incides with

$$\Delta t < \frac{2\Re(eig(D))}{|eig(D)|^2|\lambda|}. \tag{31}$$

Euler Backward

The Euler Backwards time integration method of equation (21) is given by

$$\underline{c}^{n+1} = \underline{c}^n + \Delta t A \underline{c}^{n+1} \Leftrightarrow (I - \Delta t A)\underline{c}^{n+1} = \underline{c}^n. \tag{32}$$

Since we only consider cases in which $\Re(\mu) > 0$ and $\lambda < 0$, it appears that the Euler Backward method is unconditionally stable. The use of Euler backward time integration guarantees the stability of the numerical solution. However, the use of this method gives a large discretization matrix A, which makes each time-integration step expansive, especially for more dimensional problems.

IMEX time integration

Here we assume that both D_{12} and D_{21} are non-zero. In order to combine the advantages of the stability of the Euler Backward method with the low cost per iteration step if the Euler Forward method is used, we analyze the IMEX method. If one of the cross-diffusion coefficients is zero, then the diffusion equation with the zero cross term can be integrated by the direct use of Euler Backward to obtain its concentration profile. Subsequently, this concentration can be substituted into the other diffusion equation to obtain the other concentration by the use of Euler Backward. Hence the use of IMEX is not necessary to decrease the cost per time iteration.

In the IMEX time integration we consider the implicit treatment of the terms of the diffusion matrix that are on the main diagonal and explicit treatment of the off-diagonal terms, i.e.

$$\underline{c}^{n+1} = \underline{c}^n + \Delta t \begin{pmatrix} D_{11}L & 0 \\ 0 & D_{22}L \end{pmatrix} \underline{c}^{n+1} + \Delta t \begin{pmatrix} 0 & D_{12}L \\ D_{21}L & 0 \end{pmatrix} \underline{c}^n \tag{33}$$

This time integration can be represented by

$$\underline{c}^{n+1} = \left(I - \Delta t \begin{pmatrix} D_{11}L & 0 \\ 0 & D_{22}L \end{pmatrix} \right)^{-1} \left(I + \Delta t \begin{pmatrix} 0 & D_{12}L \\ D_{21}L & 0 \end{pmatrix} \right) \underline{c}^n. \tag{34}$$

Let r and $\underline{w}$ be an eigenvalue and eigenvector of the above matrix, then we consider

$$\left(I - \Delta t \begin{pmatrix} D_{11}L & 0 \\ 0 & D_{22}L \end{pmatrix} \right)^{-1} \left(I + \Delta t \begin{pmatrix} 0 & D_{12}L \\ D_{21}L & 0 \end{pmatrix} \right) \underline{w} = r\underline{w}. \tag{35}$$

For stability, we need $|r| < 1$, and the above equation can be written as a generalized eigenvalue problem

$$\left(I + \Delta t \begin{pmatrix} 0 & D_{12}L \\ D_{21}L & 0 \end{pmatrix} \right) \underline{w} = r \left(I - \Delta t \begin{pmatrix} D_{11}L & 0 \\ 0 & D_{22}L \end{pmatrix} \right) \underline{w}. \tag{36}$$

Let $\underline{v}$ be an eigenvector of L with eigenvalue λ, then, we set $\underline{w} = (\underline{v} \quad \beta\underline{v})^T$. Since L is

symmetric its eigenvectors form a basis for $\mathbb{R}^n$, i.e. it is complete, and since $A \in \mathbb{R}^{2n\times 2n}$ the set of eigenvectors $\underline{w}$ represents a basis for $\mathbb{R}^{2n}$ if there are two distinct values for β for each eigenvector $\underline{v}$. Note that

$$\left(I + \Delta t \begin{pmatrix} 0 & D_{12}L \\ D_{21}L & 0 \end{pmatrix}\right) \begin{pmatrix} \underline{v} \\ \beta\underline{v} \end{pmatrix} = \begin{pmatrix} (1+\Delta t D_{12}\lambda\beta)\underline{v} \\ (\beta + \Delta t D_{21}\lambda)\underline{v} \end{pmatrix}, \tag{37}$$

and similarly

$$\left(I - \Delta t \begin{pmatrix} D_{11}L & 0 \\ 0 & D_{22}L \end{pmatrix}\right) \begin{pmatrix} \underline{v} \\ \beta\underline{v} \end{pmatrix} = \begin{pmatrix} (1-\Delta t D_{11}\lambda)\underline{v} \\ (\beta - \Delta t D_{22}\lambda\beta)\underline{v} \end{pmatrix}, \tag{38}$$

We search β such that the right-hand side of equation (38) is a multiple of the right-hand side of (37), here this multiple defines the eigenvalue r, hence,

$$r = r(\lambda\Delta t) = \frac{1+\Delta t D_{12}\lambda\beta}{1-\Delta t D_{11}\lambda} = \frac{\beta + \Delta t D_{21}\lambda}{\beta - \Delta t D_{22}\lambda\beta}. \tag{39}$$

The above equation gives a quadratic equation for β with solutions:

$$\beta_\pm(\xi) = \frac{D_{22} - D_{11} \pm \sqrt{(D_{12}-D_{22})^2 + 4D_{12}D_{21}(1+\xi D_{22})(1+\xi D_{11})}}{2D_{12}(1+\xi D_{22})}, \tag{40}$$

where we set $\xi := -|\lambda|\Delta t$ for ease of notation. First we consider the case $D_{12}D_{21} > 0$, and we assume that $\beta_\pm \in \mathbb{R}$, which is reasonable since $\xi < 0$. Since $\beta_\pm$ stays bounded as $\xi \to 0$, we see that $|r| \to 1$ as $\xi \to 0$. Furthermore, since

$$\lim_{\xi\to\infty} \beta_\pm = \pm\sqrt{\frac{D_{21}D_{11}}{D_{12}D_{22}}},$$

it follows that

$$\lim_{\xi\to\infty} |r| = \sqrt{\frac{D_{12}D_{21}}{D_{11}D_{22}}} < 1 \text{ if and only if } D_{12}D_{21} < D_{11}D_{22}.$$

Note that this is also a necessary and sufficient condition for $\Re(eig(D)) > 0$, which is necessary and sufficient for an analytically stable system. Now we consider solutions for ξ of

$$|r| = 1, \text{ i.e. } (1-\xi D_{12}\beta_\pm)^2 = (1+\xi D_{11})^2. \tag{41}$$

Note that $\beta_\pm$ is a function of ξ (see equation (40)). The roots of the above equation are given by

$$\xi \in \{0, \frac{-(D_{11}+D_{22}) \pm \sqrt{(D_{11}+D_{22})^2 - 4(D_{11}D_{22} - D_{12}D_{21})}}{D_{11}D_{22} - D_{12}D_{21}}\}. \tag{42}$$

The first root is not interesting and the last two roots are negative or complex-valued since $D_{11}D_{22} - D_{21}D_{12} > 0$. This implies that none of the roots is positive and we always have $|r| < 1$ if $D_{11}D_{22} - D_{12}D_{21} > 0$ and $D_{12}D_{21} > 0$ so the method is unconditionally stable. The roots in equation (42) apply for all cases when $\beta_\pm \in \mathbb{R}$. Since for this case we have that $|r| < 1$ also as $\xi \to \infty$ this implies that the chosen time integration is super-stable.

Next we consider $D_{12}D_{21} < 0$, then $\beta_\pm \in \mathbb{R}$ for small values of ξ, whereas for sufficiently large values of ξ we have $\beta_\pm \notin \mathbb{R}$ (see equation (40)). Now we treat the case that $\beta_\pm \notin \mathbb{R}$, the real-valued case was treated in the preceding paragraph where it followed that $|r| < 1$ for $D_{12}D_{21} > 0$. We obtain again that

$$\lim_{\xi \to \infty} |r| = \sqrt{\frac{|D_{12}D_{21}|}{D_{11}D_{22}}} < 1 \text{ if and only if } |D_{12}D_{21}| < D_{11}D_{22}.$$

Note that this guarantees that $\Re(eig(D)) > 0$. Again we solve $|r| = 1$, taking into account that possibly $\beta_\pm \notin \mathbb{R}$. Assuming that $\beta_\pm \notin \mathbb{R}$, we rewrite equation (39) by

$$|r|^2 = \frac{1 - 2\xi D_{12}\Re(\beta) + \xi^2|\beta|^2}{(1 + \xi D_{11})^2} = 1. \tag{43}$$

The real part and modulus of $\beta_\pm$ follow easily from equation (40). All parameters in the above equation are real-valued. A solution by MAPLE reveals the solution

$$\xi \in \{0, -\frac{D_{11} + D_{22}}{D_{11}D_{22} + D_{12}D_{21}}\}.$$

Note that the roots for the case of a real-valued β also apply, however, these roots are not treated here since they give non-positive values for ξ. The first root is not interesting, however, the second root is positive if and only if $|D_{12}D_{21}| > D_{11}D_{22}$ and $D_{12}D_{21} < 0$. This implies the following criterion for stability if $-D_{12}D_{21} > D_{11}D_{22}$:

$$\xi < -\frac{D_{11} + D_{22}}{D_{11}D_{22} + D_{12}D_{21}}.$$

Further, it can be seen that if $|D_{12}D_{21}| < D_{11}D_{22}$, then, there is no positive root and hence the method is unconditionally stable and super stable.

To summarize this all, we end up with the following theorem:

Theorem 1 *Consider the time integration of eq.* (22)*, and let* λ *be an eigenvalue of the discretized Laplace operator whose eigenvalues are all negative,* $D \in \mathbb{R}^{2\times 2}$ *and* $D_{11}, D_{22} > 0$*, and let* $\Re(eig(D)) > 0$*, then;*

1. *The explicit time integration is stable if*

$$\Delta t < \frac{2\Re(eig(D))}{|\lambda||eig(D)|^2}.$$

2. *The implicit time-integration is unconditionally stable and super stable.*

3. *If* $0 < |D_{12}D_{21}| < D_{11}D_{22}$ *then the IMEX time-integration, given in eq.* (33)*, is unconditionally stable and super stable. If* $-D_{12}D_{21} > D_{11}D_{22}$ *then the IMEX time-integration is stable if*

$$|\lambda|\Delta t < -\frac{D_{11}+D_{22}}{D_{11}D_{22}+D_{12}D_{21}}.$$

As consequences of the above assertion one can easily prove the following statements:

Corollary 1 *Let all hypotheses in Theorem 1 be satisfied, then*

1. *For all symmetric discretizations, Finite Element discretization in particular, Theorem 1 holds.*

2. *A consequence of Theorem 1 is that the IMEX time integration is unconditionally stable if the diffusion matrix is diagonally dominant and if the discretized Laplacian is symmetric (in particular for Finite Element discretization).*

As an example we present the modulus of the eigenvalue r as a function of $|\lambda|\Delta t$ for $D_{11} = 3$, $D_{22} = 1$, $D_{12} = -0.05$ and $D_{21} = -0.01$ in Figure 1. We see that that the magnitude starts at 1 and asymptotically converges towards $\sqrt{\frac{D_{12}D_{21}}{D_{11}D_{22}}}$ as $|\lambda|\Delta t \to \infty$. Moreover, the eigenvalue stays real-valued here since $\beta_\pm$ are real-valued. In the plot we use both modes for $\beta_\pm$, where mode 1 and mode 2 correspond to β_+ and β_- respectively.

Further in Figure 2, we plot the case with $D_{12} = 0.05$ and otherwise the same data, where the eigenvalue r becomes complex-valued since $\beta_\pm$ are no longer real-valued. For completeness we plot the imaginary part of the eigenvalue r for both modes in Figure 3. We see that from a certain value of $|\lambda|\Delta t$ the eigenvalues become complex. As a final example we plot the modulus of r as a function of $|\lambda|\Delta t$ for $D_{11} = 3$, $D_{22} = 1$, $D_{12} = 5$ and $D_{21} = -1$ in Figure 4. It can be seen that r decreases at the early stages and increases up to the asymptotic value $\sqrt{\frac{|D_{21}D_{12}|}{D_{11}D_{22}}} > 1$. The magnitude of the eigenvalue r becomes one at $|\lambda|\Delta t = 2$.

Numerical experiments reveal that the derived criterion in Theorem 1 is sharp.

4.2 Discretization of the Stefan problem

In this section we describe the full numerical solution of the vector-valued Stefan problems. First, we describe the discretization of the diffusion equations. Subsequently, the discrete

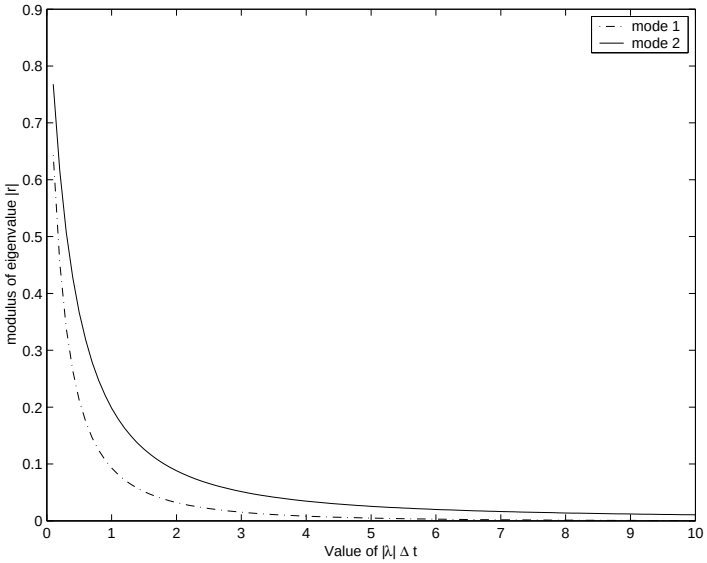

Figure 1: The modulus of the eigenvalue r as a function of $|\lambda|\Delta t$ for $D_{11} = 3$, $D_{22} = 1$, $D_{12} = -0.05$ and $D_{21} = -0.01$. Mode 1 and mode 2 correspond to β_+ and β_- respectively.

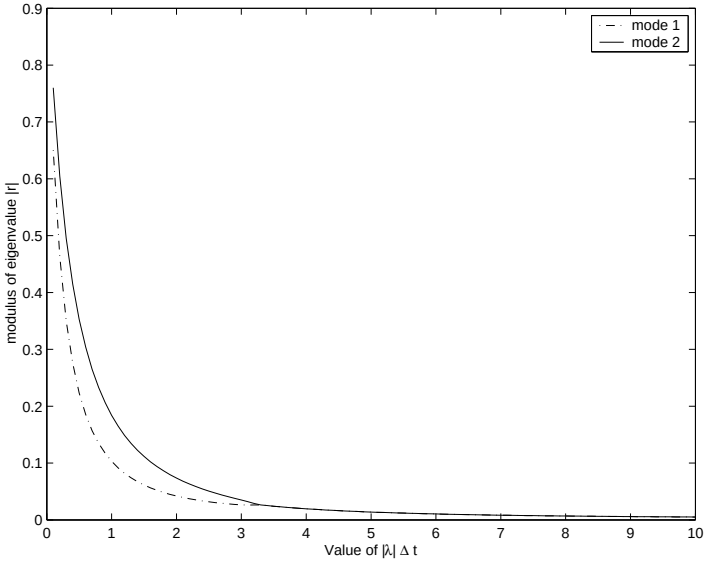

Figure 2: The modulus of the eigenvalue r as a function of $|\lambda|\Delta t$ for $D_{11} = 3$, $D_{22} = 1$, $D_{12} = 0.05$ and $D_{21} = -0.01$. Mode 1 and mode 2 correspond to β_+ and β_- respectively.

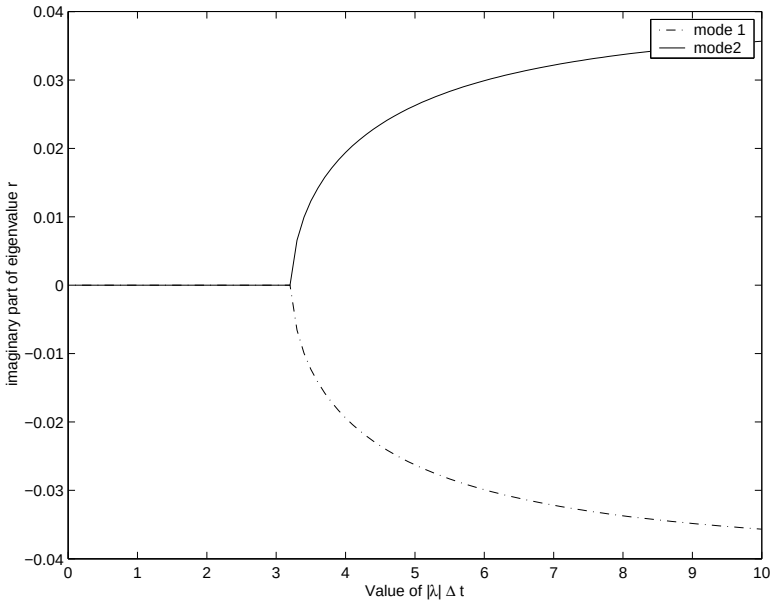

Figure 3: The imaginary part of the eigenvalue r as a function of $|\lambda|\Delta t$ for $D_{11} = 3$, $D_{22} = 1$, $D_{12} = 0.05$ and $D_{21} = -0.01$. Mode 1 and mode 2 correspond to β_+ and β_- respectively.

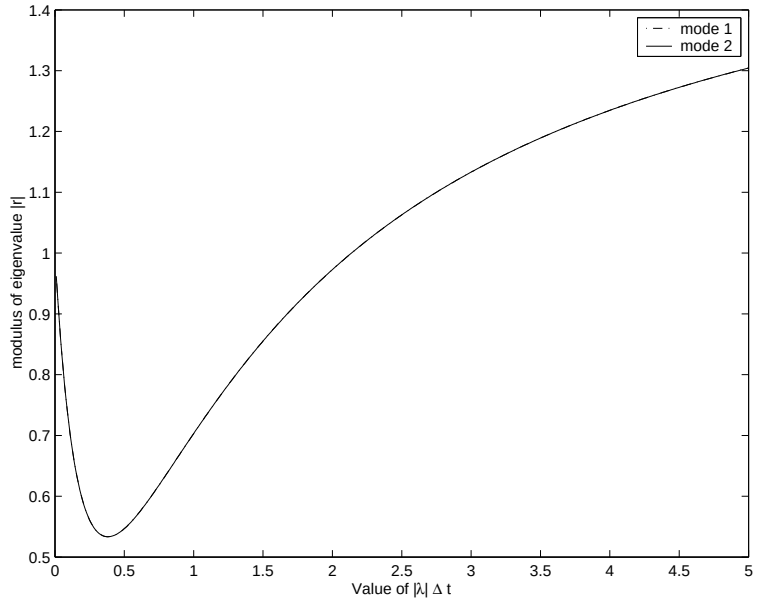

Figure 4: The modulus of the eigenvalue r as a function of $|\lambda|\Delta t$ for $D_{11} = 3$, $D_{22} = 1$, $D_{12} = 5$ and $D_{21} = -1$. Note that the two modes overlap.

boundary conditions at the moving interface and the solution procedures to solve the resulting non-linear problem are treated. Finally, the adaptation of the moving boundary is described.

Discretisation of the interior region

We use a finite difference method with a Euler Forward or backward or IMEX time integration to solve the diffusion equation in the inner region. An explicitly treated convection term due to grid-movement is included. Since the magnitude of the gradient is maximal near the moving interface we use a geometrically distributed grid such that the discretization near the interface is fine and coarse farther away from the moving interface. Furthermore, we use a virtual grid-point near the moving boundary. The distance between the virtual node and the interface is chosen equal to the distance between the interface and the first grid-node. The resulting set of linear equations is solved using a tridiagonal matrix solver.

Discrete boundary conditions at the interface

We define the discrete approximation of the concentration as $c_{i,k}^{j}$, where j, i and k respectively denote the time-step, the index of the chemical (alloying) element and gridnode. The virtual gridnode behind the moving interface and the gridnode at the interface respectively have indices $k = -1$ and $k = 0$. At the moving interface, we obtain from discretization of the Stefan condition for $i \in \{1, \ldots, n-1\}$:

$$\frac{1}{c_i^{\text{part}} - c_i^{\text{sol}}} \left\{ \sum_{j=1}^{n} D_{i,j} \frac{c_{j,1}^{k+1} - c_{j,-1}^{k+1}}{2\Delta r} \right\} = \frac{1}{c_{i+1}^{\text{part}} - c_{i+1}^{\text{sol}}} \left\{ \sum_{j=1}^{n} D_{i+1,j} \frac{c_{j,1}^{k+1} - c_{j,-1}^{k+1}}{2\Delta r} \right\}.$$

Note that the concentration profile of each element is determined by the value of the interfacial concentration. Above equation can be re-arranged into a zero-point equation for all chemical elements. All interfacial concentrations satisfy the hyperbolic relation (1). Combination of all this, gives for $i \in \{1, ..., n-1\}$ and $i = n$

$$f_i(c_1^{\text{sol}}, \ldots, c_n^{\text{sol}}) = (c_{i+1}^{\text{part}} - c_{i+1}^{\text{sol}}) \textstyle\sum_{j=1}^{n} D_{i,j}(c_{j,1}^{k+1} - c_{j,-1}^{k+1}) - (c_i^{\text{part}} - c_i^{\text{sol}}) \sum_{j=1}^{n} D_{i+1,j}(c_{j,1}^{k+1} - c_{j,-1}^{k+1}) = 0,$$

$$(c_1^{\text{sol}})^{m_1} (c_2^{\text{sol}})^{m_2} (...) (c_n^{\text{sol}})^{m_n} = K = K(T).$$

To approximate a root for the 'vector-function' $\mathbf{f}$ we use a numerical method. We compare the solution by use of the 'inaccurate Newton' method to the Picard iterations. Let $\underline{z} := (c_1^{\text{sol}}, \ldots, c_n^{\text{sol}})^T$, then

$$\underline{z}^{k+1} = \underline{z}^k - J^{-1}(\underline{z}^k)\underline{f}(\underline{z}^k),$$

where J denotes the discretized Jacobian matrix, where central differences are used for the determination of the derivatives of the first $n-1$ equations. The iteration is terminated when sufficient accuracy is reached. This is explained in more detail in [29]. Note that for each Newton iteration five evaluations of the concentration profiles are needed. Further, the initial guess must be close to the solution and the convergence of the Newton iteration scheme is quadratic. Hence, if the method converges, then convergence is fast. The Picard

iteration scheme is based on

$$\underline{z}^{k+1} = \underline{g}(\underline{z}^k),$$

where the vector-function $\underline{g}$ is defined as:

$$c_1^{\mathrm{sol}} = g_1 := \frac{K}{(c_1^{\mathrm{sol}})^{m_1-1}(c_2^{\mathrm{sol}})^{m_2}(...)(c_n^{\mathrm{sol}})^{m_n}},$$

$$c_{i+1}^{\mathrm{sol}} = g_{i+1} := c_{i+1}^{\mathrm{part}} - \frac{(c_i^{\mathrm{part}} - c_i^{\mathrm{sol}})\sum_{j=1}^{n} D_{i+1,j}(c_{j,1}^{k+1} - c_{j,-1}^{k+1})}{\sum_{j=1}^{n} D_{i,j}(c_{j,1}^{k+1} - c_{j,-1}^{k+1})}, \quad i \in \{1,\ldots,n-1\}.$$

A disadvantage of the Picard-iteration scheme is that the convergence is linear. However, only one evaluation of the concentration profile is needed per iteration, hence cost per iteration is reduced five times. A criterion for convergence of the Picard iterations is that the spectral radius of the Jacobian of the function $\underline{g}$ should be less than one. For large Δt we observed that the spectral radius becomes larger than one. For these cases a Picard iteration scheme with relaxation is used, then

$$\underline{z}^{k+1} = \underline{z}^k + \omega(\underline{g}(\underline{z}^k) - \underline{z}^k),$$

where ω is the relaxation parameter. For some $\omega > 0$ a slightly better convergence is obtained, although not for all $0 < \omega < 1$ the improvement is significant. Further, we see that the error, defined by $||\underline{z}^{k+1} - \underline{z}^k||_2$, never gets less than 10^{-6} within 20 iterations.

Adaptation of the moving boundary

The moving interface is adapted according to the stefan condition. In [28] the forward (explicit) Euler and Trapezium time integration methods are described and compared. It was found that the (implicit) Trapezium method was superior in accuracy. Furthermore, the iteration step to determine the interfacial concentrations is included in each Trapezium step to determine the interfacial position. Hence, the work per time-iteration remains the same for both time-integration methods. Therefore, the Trapezium rule is used to determine the interfacial position as a function of time. We terminate the iteration when sufficient accuracy is reached, i.e. let ε be the inaccuracy, then we stop the iteration when the inequality

$$\sum_{i=1}^{n} |u_i^{\mathrm{s}}(p+1) - u_i^{\mathrm{s}}(p)| + \frac{|S^{j+1}(p+1) - S^{j+1}(p)|}{S^{j+1} - M} < \varepsilon$$

holds. Here S^j denotes the discrete approximation of the interfacial position at time-step j. The integer p represents the iteration number during the determination of the interfacial concentrations and position. We finally remark that a numerical solution for diffusion in ternary alloys including cross-diffusion for fixed boundaries can be found in Naumann and Savoca [18].

4.3 Diagonalization of the diffusion matrix

First the eigenvalues and eigenvectors of the diffusion matrix are computed for the transformation of the concentration. The particle concentrations are also transformed and the hyperbolic relation between the interfacial concentrations changes. A great advantage of the diagonalization argument is that a fully implicit method, which is unconditionally stable, can be used easily to integrate the concentration profile in time. However, the eigenvalues and eigenvectors should be determined at each time-step when the diffusion matrix is not constant. Further, if the diffusion matrix varies over the domain of computation, then the method is no longer applicable.

Using the diagonalization argument gives that the discrete boundary conditions at the interface change into:

$$\frac{\lambda_i}{u_i^{\text{part}} - u_i^{\text{s}}} \frac{u_{i,1}^{j+1} - u_{i,-1}^{j+1}}{2\Delta r} = \frac{\lambda_{i+1}}{u_{i+1}^{\text{part}} - u_{i+1}^{\text{s}}} \frac{u_{i+1,1}^{j+1} - u_{i+1,-1}^{j+1}}{2\Delta r}, \text{ for } j \in \{1, ..., n-1\},$$

hence

$$f_i(u_{i,0}^{j+1}, u_{i+1,0}^{j}) := \lambda_i(u_{i,1}^{j+1} - u_{i,-1}^{j+1})(u_{i+1}^{\text{part}} - u_{i+1}^{\text{s}}) - \lambda_{i+1}(u_{i+1,1}^{j+1} - u_{i+1,-1}^{j+1})(u_i^{\text{part}} - u_i^{\text{s}}) = 0$$

$$f_n(u_1^{\text{s}}, ..., u_n^{\text{s}}) := (\sum_{j=1}^{n} p_{1j} u_j^s)^{m_1} (\sum_{j=1}^{n} p_{2j} u_j^s)^{m_2} (\ldots) (\sum_{j=1}^{n} p_{nj} u_j^s)^{m_n} - K = 0.$$

For the determination of the interface position, one uses the Stefan condition obtained after diagonalization. The method becomes similar to the method described in [29].

5 Numerical experiments

First we present a comparison between the analytical solution and the numerical solution by the use of the diagonalization argument and Newton iterations. Subsequently, the various numerical solution techniques are compared.

5.1 Numerical solutions and analytical solutions

As a numerical experiment we show the computation of the dissolution of a planar phase for the case that the diffusion matrix is diagonalizable. Furthermore, we compare the computed numerical solutions with the self-similar solution as developed in Section 3. As input-data we used

$$\underline{c}^0 = (0, 0)^T, \qquad \underline{c}^{\text{part}} = (50, 50)^T,$$

$$D = \begin{pmatrix} 1 & -1/2 \\ 1/4 & 2 \end{pmatrix}, \qquad K = 1.$$

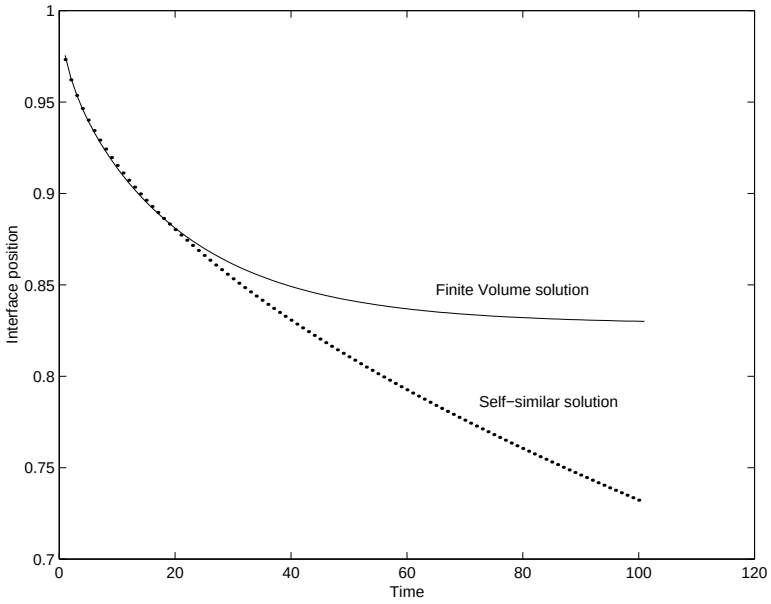

Figure 5: The interfacial position as a function of time. The dotted curve corresponds to self-similar solution and the other curve corresponds to the numerical approach.

The above matrix is diagonalizable. In Figure 5 we plot the interface as a function of time for the self-similar solution and numerical solution, which was obtained by the use of diagonalization and Newton iterations. As to be expected the solutions co-incide for small times and start to deviate for later stages. From Figure 5 it is concluded that the numerical scheme is applicable for cross-diffusion. We further show the interface position as a function of time for the self-similar (exact) solution and the quasi-binary approach in Figure 6. It can be seen that the quasi-binary approach is very accurate for this case.

Subsequently, we show the interfacial position as a function of time for the case that the diffusion matrix is not diagonalizable in Figure 7. The data-set that we used is given by:

$$\underline{c}^0 = (0,0)^T, \qquad \underline{c}^{\text{part}} = (100,50)^T,$$

$$D = \begin{pmatrix} 2 & -1 \\ 1 & 2 \end{pmatrix}, \qquad K = 1.$$

We show the results for the exact solution, see Section 4.3. and the results for the asymptotic approximation (i.e. the quasi-binary approach), see Section 4.4. It can be seen that the curves co-incide well and hence for this case the asymptotic approach is accurate.

5.2 Comparison of the numerical methods

In this section we compare the performance of several numerical techniques. First we distinguish between the IMEX and fully implicit time integration methods for the coupled

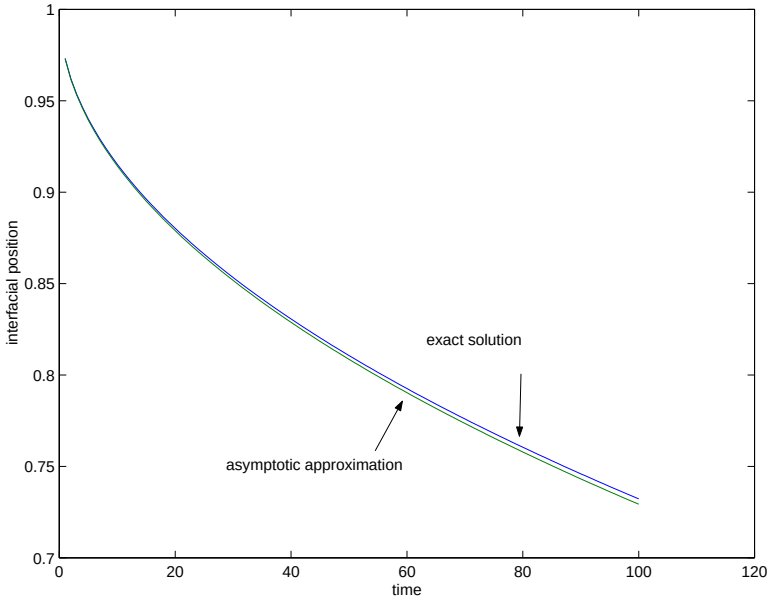

Figure 6: The interfacial position as a function of time for the same dataset as in Figure 5 for the exact self-similar solution and the asymptotic approximation (quasi binary approach).

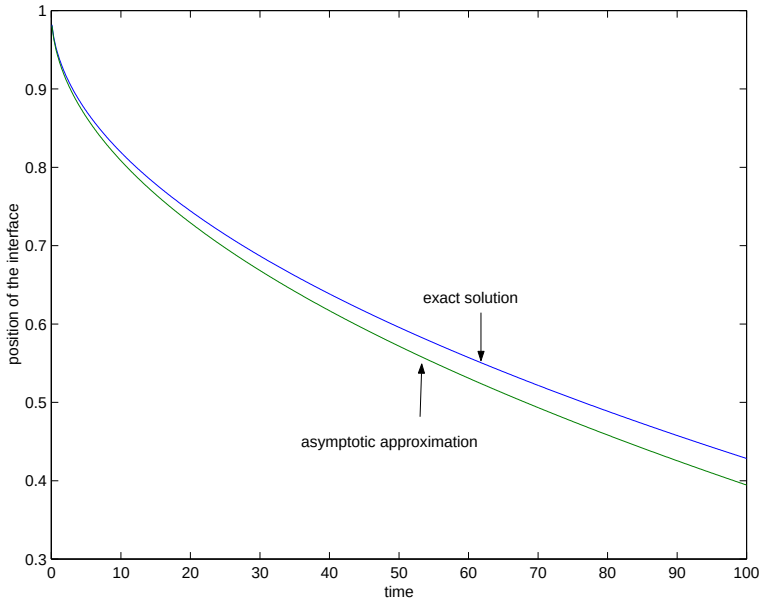

Figure 7: The interface position as a function of time for the case that the diffusion matrix is not diagonalizable. The exact- and asymptotic solution are shown.

set of equations. For both time integrations we analyze the performance of the Newton and Picard iterations to solve the non-linear problem. Finally, we compare these solutions with those that were obtained by the use of the diagonalization argument. As a test-problem we take

$$D = \begin{pmatrix} 1 & -0.25 \\ -0.25 & 2 \end{pmatrix} \qquad \underline{c}^p = \begin{pmatrix} 50 \\ 50 \end{pmatrix} \qquad c_1^{\text{sol}} c_2^{\text{sol}} = 1 \qquad \underline{c}^0 = \begin{pmatrix} 0 \\ 0 \end{pmatrix}.$$

For the above configuration the IMEX time integration of the concentration profiles should be unconditionally stable with respect to the time-step according to Theorem 1.

5.2.1 The IMEX time integration

Note that the proof of Theorem 1 has been given for the case that the interface position does not change in time. From the numerical simulations it turned out that convergence to the solution of the non-linear problem depends on the choice of the time-step and the grid-size. In Table 1 we present the CPU time for the Newton, Picard (with and without relaxation) for time-steps $\Delta t = 0.1$ and $\Delta t = 1$. The CPU-time is at $t = 100$. The number of iterations is for the numerical solution of the non-linear problem at the second time-step. All values in Table 1 are for the IMEX time integration. The numbers 0.5 and 1.5 denote the value of ω used in the relaxated Picard method.

Table 1: CPU-times and number of iterations for the numerical solution of the non-linear problem for a grid of 50 gridnodes.

method / convergence	CPU-time ($\Delta t = 0.1$)	CPU-time ($\Delta t = 1$)
IMEX-Newton	12.08	-
IMEX-Picard	3.36	-
IMEX-Picard (0.5)	3.47	1.33*
IMEX-Picard (1.5)	3.13	-

* inaccurate solution

From Table 1 it can be seen that Newton's method takes most CPU-time. This is caused by the fact that for each time iteration we need to evaluate the concentration profiles five times. Further, it turns out that the IMEX method performs badly when the time-step is enlarged. The minus-bars in Table 1 denote that the method did not converge (for the Picard method) or converged to a wrong solution (Newton). Convergence to the wrong solution in the Newton case could not be avoided by the choice of a better initial guess for the interface concentrations. For the Picard method, this is attributed to the fact that the spectral radius of the Jacobian of the function $\underline{g}$ in the Picard method becomes larger than one. We remark that the solution can be determined numerically for large Δt by means of relaxation of Picard's method. However, we recommend here to choose a small time-step Δt instead, since it is not easy to obtain an optimal choice for ω for different values of Δt and Δx.

5.2.2 The Euler Backward time integration

We remark that this method is unconditionally stable, see Theorem 1. In Table 2 we present the number of iterations for the solution of the non-linear problem and CPU-time for the Newton, Picard (with relaxation) methods for time-steps $\Delta t = 0.1$ and $\Delta t = 1$. The CPU-time is at $t = 100$. All values in Table 2 are for the fully implicit time-integration.

Table 2: CPU-times and number of iterations for the numerical solution of the non-linear problem for a grid of 50 gridnodes.

method / convergence	CPU-time ($\Delta t = 0.1$)	CPU-time ($\Delta t = 1$)
Euler Backward-Newton	88.82	8.88
Euler Backward-Picard	4.41	1.15
Euler Backward-Picard (0.5)	20.88	3.61
Euler Backward-Picard (1.5)	13.92	2.14

From Table 2 we see that Picard's method is faster than the Newton method. This agrees with the observation for the IMEX time-integration. Further, we see that for $\Delta t = 0.1$ the IMPLICIT method takes more CPU-time than the IMEX scheme. However, for large time-steps it turns out that the Euler Backward method is more reliable than the IMEX method method. Picard (without relaxation) seems to give the best results. For reasons of robustness the IMPLICIT method is favorable over the IMEX method. However, for CPU-time and small time-step we prefer to use the IMEX method. Although the speed-up of the IMEX method compared to the Euler Backward method does not seem to be very significant for the Picard iterations compared to the Newton iterations.

5.2.3 Computation times of the IMEX and Euler Backward methods

From the above it seems that the Euler Backward method is advantageous. Since we intend to extend the models to more dimensions as well, we present some CPU-times for 10 time-iterations for a two-dimensional diffusion equations. The discretization is done on an equidistant grid with the use of Finite Volumes. Furthermore, the values of the interfacial concentrations are prescribed $c_1^{\text{sol}} = 1 = c_2^{\text{sol}}$ and the boundaries are fixed. The calculations are done by the use of an IMEX and Euler Backward time integration. The linear system of equations has been solved by Gaussian elimination for all cases. The results are presented in Table 3.

Table 3: Calculation times for 10 time iterations

method / grid	25×25	50×50	100×100	200×200
IMEX	0.1500	0.8500	5.7700	46.5700
Euler Backward	0.2800	1.6900	14.0400	116.9400

From Table 3 it can be seen that the IMEX method requires less CPU-time than the Euler Backward method. The difference increases as the number of gridnodes increases. This is a consequence of the fact that the overall discretization matrix of the Euler Backward method gets larger and gets a larger bandwidth. For three-dimensional problems with many more gridnodes, this difference is expected to increase. Hence, for small time-steps, we prefer the use of the IMEX method.

5.2.4 Use of diagonalization of the diffusion matrix

Until now we observed that the Euler Backward method is more robust than the IMEX method, but the solution of the linear system of equations takes more time, especially when the number of spatial dimensions increases. If the diagonalization argument is used then the IMEX method and Euler Backward method are equivalent and hence both efficiency from IMEX and robustness of the Euler Backward are obtained. The CPU-times and number of iterations are listed in Table 4.

Table 4: CPU-times and number of iterations for the numerical solution of the non-linear problem for a grid of 50 gridnodes.

method / convergence	CPU-time ($\Delta t = 0.1$)	CPU-time ($\Delta t = 1$)
DIAG-Newton	11.22	1.12
DIAG-Picard	2.94	1.01
DIAG-Picard (0.5)	3.00	1.17
DIAG-Picard (1.5)	3.01	0.88

We see from Table 4 that Picard's method gives the shortest CPU-time. Further, we see that this method is efficient (shortest computation times for both $\Delta t = 0.1$ and $\Delta t = 1$) and robust. Therefore, we recommend the use of the diagonalization argument of the diffusion matrix and the Picard iterations for the non-linear problem. We note that whenever the diffusion matrix varies over the domain of computation, which is the case when diffusion is non-linear, then the diagonalization argument is not applicable. However, if the diffusion matrix is only a function of time, then the diagonalization argument is very beneficial. Note that then at each time-step the concentrations should be transformed.

Furthermore, if the matrix is not diagonalizable, the diffusion matrix can be transformed to a Jordan matrix to uncouple some of the diffusion equations. This can also give a speed-up. Then, a choice between the IMEX and Euler Backward time integration can be made.

Remark: In the numerical experiments we observed that the number of iterations is smaller for the Newton method than for the Picard iterations. However, the CPU-time is higher for Newton iterations since each Newton iteration requires multiple evaluation of the concentration profiles. Further, it was observed that the dependence of the convergence on the time-step is larger for the Newton iterations than for the Picard iterations.

6 Conclusions

A model, based on a vector-valued Stefan problem, has been developed to predict dissolution kinetics of stoichiometric particles in multi-component alloys. Cross-diffusion of the alloying elements is taken into account, which gives a strong coupling of the differential equations. Using a diagonalization argument the vector-valued Stefan problem with cross-diffusion is transformed into a vector-valued Stefan problem where the cross-terms vanish whenever the diffusion matrix is diagonalizable. If the diffusion matrix is not diagonalizable, the Jordan decomposition is used to facilitate the analysis. The hyperbolic relation between the interfacial concentrations becomes more complicated, however, since the eigenvectors of the diffusion matrix have to be taken into account as well. In spite of this complication, the vector-valued Stefan problem can be approximated by a quasi-binary in a similar way as for the case in which no cross-diffusion is taken into account for the vector-valued Stefan problem. Similar as in the case of no cross-diffusion we obtain expressions for the effective interfacial concentration, particle concentration and effective diffusion coefficient.

Further, we analyzed several numerical methods for the cross-diffusion problem with the moving interface. We analyze the Euler Backward time integration method, which is proven to be unconditionally stable. This method turns out to be very robust when it is used in the solution of the non-linear system to determine the interfacial concentrations. A drawback is the long computation time needed to solve the large system of linear equations from the discretization. This becomes worse as the dimensionality of the problem increases. The IMEX time-integration method to integrate the concentration profiles as a function of time is conditionally stable under the circumstance that $-D_{12}D_{21} > D_{11}D_{22} > 0$ and for other cases the method is unconditionally stable. However, it turns out the method is less robust when a large time-step is used. Although, the computation times are less than for the fully implicit method. If diagonalization is used then the IMEX and Euler Backward time-integration methods are equivalent. Then, stability is guaranteed and the discretization (stiffness) matrix conserves its original sparsity pattern (A and L have the same sparsity). Hence, the method is efficient. If the diffusion matrix is constant over the domain of computation (such as for non-linear diffusion), then the diagonalization argument is no longer applicable. Further, if the diffusion matrix depends on time only, then the diagonalization has to be carried out at each time-step. Since D is a small sized matrix in general, this does not restrict its applicability.

Acknowledgment

We wish to express our gratitude to prof.dr.ir. S. van der Zwaag from the department of aerospace engineering at the Delft University of Technology for drawing our attention to this problem.

References

[1] H.B. Aaron and G.R. Kotler. Second phase dissolution. *Metallurgical transactions*, 2:1651–1656, 1971.

[2] C. Atkinson, T. Akbay, and R.C. Reed. Theory for reaustenization from ferrite/cementite mixtures in fe-c-x steels. *Acta Materialia*, 43 (5):2013–2032, 1995.

[3] U.L. Baty, R.A. Tanzilli, and R.W. Heckel. Dissolution kinetics of $CuAl_2$ in an Al-4Cu alloy. *Metallurgical Transactions*, 1:1651–1656, 1970.

[4] G. Birkhoff and S. MacLane. *A survey of modern algebra*. Macmillan, New York, 1953.

[5] J. Chadam and H. Rasmussen. *Free boundary problems involving solids*. Longman, Scientific & technical Harlow, 1993.

[6] S. Chen, B. Merriman, S. Osher, and P. Smereka. A simple level-set method for solving stefan problems. *J. Comp. Phys.*, 135:8–29, 1997.

[7] S.P. Chen, M.S. Vossenberg, F.J. Vermolen, J. van de Langkruis, and S. van der Zwaag. Dissolution of β particles in an Al-Mg-Si alloy during DSC-runs. *Materials science and engineering*, A272:250–256, 1999.

[8] J. Crank. *Free and moving boundary problems*. Clarendon Press, Oxford, 1984.

[9] U. Grafe, B. Böttger, J. Tiaden, and S.G. Fries. Coupling of multicomponent thermodynamics to a phase field model: application to solidification and solid-state transformations of superalloys. *Scripta Materialia*, 42:1179–1186, 2000.

[10] J. Ågren. Diffusion in phases with several components and sublattices. *Journal of physical chemistry of solids*, 43:421–430, 1981.

[11] R. Hubert. Modelisation numerique de la croissance et de la dissolution des precipites dans l'acier. *ATB Metallurgie*, 34-35:4–14, 1995.

[12] F.V. Nolfi jr., P.G. Shewmon, and J.S. Foster. The dissolution and growth kinetics of spherical particles. *Transactions of the metallurgical society of AIME*, 245:1427–1433, 1969.

[13] J.S. Kirkaldy and D.J. Young. *Diffusion in the condensed state*. The institute of metals, London, 1987.

[14] R. Kobayashi. Modeling and numerical simulations of dendritic crystal growth. *Physics D*, 63:410–423, 1993.

[15] G.P. Krielaart. *Primary ferrite formation from supersaturated austenite*. Thesis, Delft University of Technology, The Netherlands, 1995.

[16] P. Lancaster. *Theory of Matrices*. 2. Acad. Press, Orlando, 1985.

[17] W.D. Murray and F. Landis. Numerical and machine solutions of transient heat conduction problems involving freezing and melting. *Transactions ASME (C), Journal of heat transfer*, 245:106–112, 1959.

[18] E.B. Naumann and J. Savoca. An engineering approach to an unsolved problem in multi-component diffusion. *AICHE Journal*, 47(5):1016–1021, 2001.

[19] S. Osher and J.A. Sethian. Fronts propagating with curvature-dependent speed: Algorithms based on Hamilton-Jacobi formulations. *J. Comp. Phys.*, 79:12–49, 1988.

[20] M.H. Protter and H.F. Weinberger. *Maximum principles in differential equations*. Prentice-Hall, Englewood Cliffs, 1967.

[21] O. Reiso, N. Ryum, and J. Strid. Melting and dissolution of secondary phase particles in AlMgSi-alloys. *Metallurgical transactions A*, 24A:2629–2641, 1993.

[22] G. Segal, C. Vuik, and F.J. Vermolen. A conserving discretisation for the free boundary in a two-dimensional Stefan problem. *Journal of Computational Physics*, 141:1–21, 1998.

[23] U.H. Tundal and N. Ryum. Dissolution of particles in binary alloys: Part i: computer simulations. *Metallurgical Transactions*, 23A:433–449, 1992.

[24] Y. van Leeuwen. *Moving Interfaces in low-carbon steel*. Thesis, Delft University of Technology, The Netherlands, 2000.

[25] W. van Til, C. Vuik, and S. van der Zwaag. An inventory of numerical methods to model solid-solid phase transformations in aluminium alloys. *NIMR-report number P.004.001*, 2000.

[26] F.J. Vermolen and S. van der Zwaag. A numerical model for the dissolution of spherical particles in binary alloys under mixed mode control. *Materials science and engineering A*, 220:140–146, 1996.

[27] F.J. Vermolen, P. van Mourik, and S. van der Zwaag. An analytical approach to particle dissolution in binary alloys. *Materials science and technology*, 13:308–313, 1997.

[28] F.J. Vermolen and C. Vuik. A numerical method to compute the dissolution of second phases in ternary alloys. *Journal of computational and applied mathematics*, 93:123–143, 1998.

[29] F.J. Vermolen and C. Vuik. A mathematical model for the dissolution of particles in multi-component alloys. *Journal of computational and applied mathematics*, 126:233–254, 2001.

[30] F.J. Vermolen, C. Vuik, and S. van der Zwaag. The dissolution of a stoichiometric second phase in ternary alloys: a numerical analysis. *Materials science and engineering*, A246:93–103, 1998.

[31] F.J. Vermolen, C. Vuik, and S. van der Zwaag. A mathematical model for the dissolution kinetics of Mg_2Si phases in Al-Mg-Si alloys during homogenisation under industrial circumstances. *Materials science and engineering*, A254:13–32, 1998.

[32] F.J. Vermolen, C. Vuik, and S. van der Zwaag. A mathematical model for the dissolution of stoichiometric particles in multi-component alloys. Department of Applied Mathematical Analysis 01-01, Delft University of Technology, Delft, The Netherlands, 2001.

[33] A. Visintin. *Models of phase transitions*. Progress in nonlinear differential equations and their application: 38 Birkhauser, Boston, 1996.

[34] C. Vuik, G. Segal, and F.J. Vermolen. A conserving discretisation for a Stefan problem with an interface reaction at the free boundary. *Journal of computation and visualisation in science*, 3:109–114, 2000.

[35] M.J. Whelan. On the kinetics of particle dissolution. *Metals Science Journal*, 3:95–97, 1969.